INTERNATIONAL JOURNAL FOR NUMERICAL METHODS IN FLUIDS
Int. J. Numer. Meth. Fluids 2001; **35**: 341–356

An implicit numerical algorithm for solving non-hydrostatic free-surface flow problems

M. M. Namin, B. Lin* and R. A. Falconer

Cardiff School of Engineering, Cardiff University, Cardiff, U.K.

SUMMARY

Details are given of the development of a two-dimensional vertical numerical model for simulating unsteady free-surface flows, using a non-hydrostatic pressure distribution. In this model, the Reynolds equations and the kinematic free-surface boundary condition are solved simultaneously, so that the water surface elevation can be integrated into the solution and solved for, together with the velocity and pressure fields. An efficient numerical algorithm has been developed, deploying implicit parameters similar to those used in the Crank–Nicholson method, and generating a block tri-diagonal algebraic system of equations. The model has been applied to simulate a range of unsteady flow problems involving relatively strong vertical accelerations. The results show that the numerical algorithm described is able to produce accurate predictions and is also easy to apply. Copyright © 2001 John Wiley & Sons, Ltd.

KEY WORDS: free-surface flow; hydrodynamic modelling; non-hydrostatic pressure distribution; numerical algorithm

1. INTRODUCTION

Numerical models are now widely used for simulating flow and water quality problems in river, estuarine and coastal waters. With the rapid increase in computer power in recent years, three-dimensional hydrodynamic and water quality models are increasingly being developed for such free-surface flow problems. The main difficulty in developing such a model for unsteady flow conditions, such as tidal flows and short period waves, is that the moving free-surface forms the upper boundary of the computational domain; however, its position also constitutes a part of the solution yet to be defined. Most of the current three-dimensional unsteady free-surface flow models in the literature are based on the assumption that the vertical acceleration is small in comparison with other acceleration terms in the governing equation. Thus, a hydrostatic pressure distribution is assumed in the vertical plane [1–3]. For many applications in shallow water flows, the use of a hydrostatic pressure assumption can

* Correspondence to: Cardiff School of Engineering, Cardiff University, Queen's Building, The Parade, PO Box 686, Cardiff, CF2 3TB, U.K.

Received August 1999
Revised February 2000

produce reliable predictions of the velocity distribution. However, for a range of applications involving conditions, such as rapid bed slope changes, strong stratification or short period waves, etc., the assumption of a hydrostatic pressure distribution is no longer valid. More recently, efforts have been made to develop free-surface flow models using the non-hydrostatic pressure distribution assumption. Stansby and Zhou [4] developed a two-dimensional vertical flow model for simulating the non-hydrostatic problem, using a semi-implicit time stepping method. Casulli and Stelling [5] developed a three-dimensional quasi-hydrostatic model, in which the pressure terms were decomposed into a hydrostatic component and a hydrodynamic component and they were solved in separate steps and then summed.

Numerical models developed for predicting the moving free-surface elevations can be generally classified into two categories, i.e. the volume of fluid (VOF) method and the sigma transformation method. The VOF method is based on the concept of only a fractional volume of the surface cell being occupied by fluid [12], with this method being mainly used for simulating flows involving short period free-surface waves [6]. This method has severe stability restrictions, however, which inhibit it from being applied to problems with a large computational domain. The method of sigma co-ordinate transformation is generally used for those applications in which the free-surface elevation is nearly horizontal [2]. In this method, the water column is divided into the same number of layers, irrespective of any variations in the local water depth.

In order to solve the Reynolds equations for free-surface flow problems, it is first necessary to introduce special treatments for the incompressible condition. Pressure correction methods, such as SIMPLE, are very popular and widely used for internal flow problems. Attempts have also been made to utilize this method to model free-surface flows [7,8], but so far little progress has been made in applying this method to practical unsteady free-surface flow problems.

This paper gives details of the development of a new implicit numerical algorithm for solving the two-dimensional free-surface flow problem in the vertical plane. With this algorithm, the kinematic free-surface boundary condition is solved simultaneously with the momentum and continuity equations, so that the water elevation can be obtained along with the velocity and pressure fields as a part of the solution. Details of the model application to flow problems involving relatively strong vertical accelerations are also given, with the model being shown to give accurate and realistic predictions.

2. MATHEMATICAL FORMULATION

The governing equations used to describe the two-dimensional vertical, incompressible flows are the continuity and momentum equations, with the conservative form of these equations being expressed as follows:

$$\frac{\partial u}{\partial x}+\frac{\partial w}{\partial z}=0 \tag{1}$$

$$\frac{\partial u}{\partial t}+\frac{\partial (u^2)}{\partial x}+\frac{\partial (uw)}{\partial z}+\frac{1}{\rho}\frac{\partial p}{\partial x}=\frac{1}{\rho}\left(\frac{\partial \tau_{xx}}{\partial x}+\frac{\partial \tau_{xz}}{\partial z}\right) \tag{2}$$

$$\frac{\partial w}{\partial t}+\frac{\partial(uw)}{\partial x}+\frac{\partial(w^2)}{\partial z}+\frac{1}{\rho}\frac{\partial p}{\partial z}=\frac{1}{\rho}\left(\frac{\partial \tau_{xz}}{\partial x}+\frac{\partial \tau_{zz}}{\partial z}\right)-g \tag{3}$$

where t is time; x, z are Cartesian co-ordinates in the vertical plane; u, w are components of velocity in the x-, z-directions respectively; p is pressure; ρ is the density of water; g is the gravitational acceleration; and τ_{xx}, τ_{xz}, τ_{zx} and τ_{zz} are components of the stress tensor in the x–z plane.

If no density variation is considered, then the pressure terms in Equations (2) and (3) may be changed to $\partial P/\partial x$ and $\partial P/\partial z$ respectively, where P is defined as

$$P=\frac{p}{\rho} \tag{4}$$

A turbulence model is required to represent the turbulence stress terms in the momentum equations (2) and (3). In this paper, Prandtl's mixing length hypothesis has been used, with the internal shear stresses being given as

$$\tau_{ij}=\mu\left(\frac{\partial u_i}{\partial x_j}\right), \quad i=1,2; \quad j=1,2 \tag{5}$$

with

$$\mu=\rho l^2 J \tag{6}$$

where l is the mixing length, and, for the two-dimensional vertical hydrodynamic model, J is defined as [13]

$$J^2=2\left(\frac{\partial u}{\partial x}\right)^2+2\left(\frac{\partial w}{\partial z}\right)^2+\left(\frac{\partial u}{\partial z}+\frac{\partial w}{\partial x}\right)^2 \tag{7}$$

Substituting from Equations (4) and (5) into Equations (2) and (3) gives the two-dimensional vertical momentum equations as

$$\frac{\partial u}{\partial t}+\frac{\partial(u^2)}{\partial x}+\frac{\partial(uw)}{\partial z}+\frac{\partial P}{\partial x}=\frac{\partial}{\partial x}\left(\mu\frac{\partial u}{\partial x}\right)+\frac{\partial}{\partial z}\left(\mu\frac{\partial u}{\partial z}\right) \tag{8}$$

$$\frac{\partial w}{\partial t}+\frac{\partial(uw)}{\partial x}+\frac{\partial(w^2)}{\partial z}+\frac{\partial P}{\partial z}=\frac{\partial}{\partial x}\left(\mu\frac{\partial w}{\partial x}\right)+\frac{\partial}{\partial z}\left(\mu\frac{\partial w}{\partial z}\right)-g \tag{9}$$

3. DESCRIPTION OF PROPOSED ALGORITHM

The sigma co-ordinate system is a special type of boundary fitting co-ordinate system, which fits the vertical direction of the physical domain. In a sigma co-ordinate system one may divide

the total water depth into equi-distant vertical intervals (Figure 1(a)) or non-equal intervals (Figure 1(b)). For these types of grids, any change in the water elevation will result in a change in the grid size over all vertical intervals. In this paper, a modified sigma co-ordinate system has been developed in which the change in grid size occurs only within the upper part of the computational domain, with the grid sizes in the lower part of the vertical domain being kept constant (Figure 1(c)). The interface between these two sets of layers may have any shape, although a straight horizontal interface was used in this study.

3.1. General form of discretization

A staggered grid system was used in this model in which the velocity components were located at the centre of the sides of a grid cell, and with the pressure and all other terms being located at the centre of the cell, as shown in Figure 2. For a typical cell i, j, the continuity equation (1) was discretized implicitly in the following manner:

$$w_{i,j+1/2}^{n+1} = \sum_{k=1}^{j} c1_{j,k} u_{i-1/2,k}^{n+1} + \sum_{k=1}^{j} c2_{j,k} u_{i+1/2,k}^{n+1} + c3_j \tag{10}$$

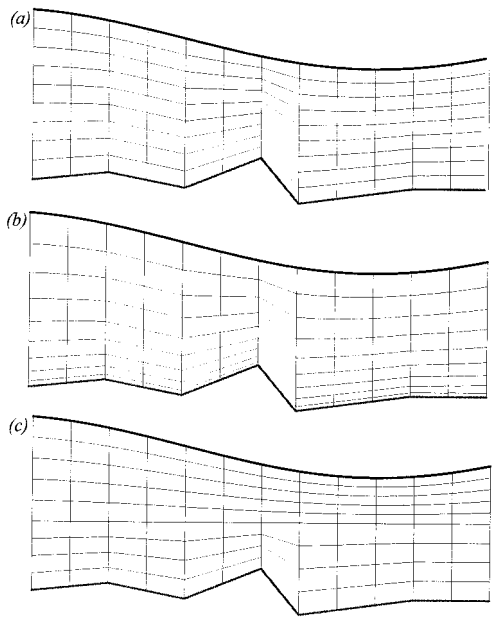

Figure 1. Three possible configurations for sigma co-ordinate system: (a) sigma co-ordinate system with uniform grid size over depth; (b) sigma co-ordinate system with non-uniform grid size over depth; (c) sigma co-ordinate system with different definitions for grid size of five upper layers and four lower layers. Size of first group varies with time, whereas the others remain unchanged.

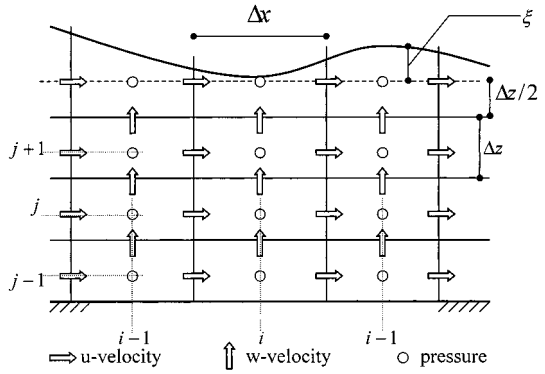

Figure 2. Location of variables and grid layout.

where n is the time step number (i.e. $n\Delta t$), and $c1$, $c2$ and $c3$ are constants. It can be seen that the vertical velocity is evaluated from the horizontal velocities in the adjacent columns. At the top layer, the continuity equation can be rearranged to determine the water elevation accordingly

$$\xi_i^{n+1} = \sum_{k=1}^{nj} c4_k u_{i-1/2,k}^{n+1} + \sum_{k=1}^{nj} c5_k u_{i+1/2,k}^{n+1} + c6 \tag{11}$$

where $c4$, $c5$ and $c6$ are constants, nj is the total number of vertical layers.

The momentum equations (8) and (9) were also discretized implicitly, and written in the following general forms:

$$\sum_{k=1}^{nj} a1_{j,k} u_{i-1/2,k}^{n+1} + \sum_{k=1}^{nj} b1_{j,k} P_{i,k}^{n+1} + \sum_{k=1}^{nj} a2_{j,k} u_{i+1/2,k}^{n+1} + \sum_{k=1}^{nj} b2_{j,k} P_{i+1/2,k}^{n+1} + \sum_{k=1}^{nj} a3_{j,k} u_{i+3/2,k}^{n+1} = d_{0j} \tag{12}$$

$$(e_1 w_{j-1/2}^{n+1} + e_2 P_j^{n+1} + e_3 w_{j+1/2}^{n+1} + e_4 P_{j+1}^{n+1} + e_5 w_{j+3/2}^{n+1}) + \sum_{k=1}^{nj} g1_k u_{i-1/2,k}^{n+1} + \sum_{k=1}^{nj} g2_k u_{i+1/2,k}^{n+1} = e_0 \tag{13}$$

3.2. Elimination of pressure terms

The pressure term within the top layer was defined using the following hydrostatic representation:

$$P_{i,nj}^{n+1} = g\xi_i^{n+1} + P_a/\rho \tag{14}$$

where P_a is atmospheric pressure acting on the water surface. By substituting Equation (11) into Equation (14), the pressure in the top layer can be evaluated in terms of the neighbouring horizontal velocity components only. Likewise, if Equation (10) is substituted into Equation (13), an equation containing $P_{i,j}^{n+1}$, $P_{i,j-1}^{n+1}$ can be derived together with the same horizontal velocity components. Thus, having $P_{i,nj}^{n+1}$ expressed using the neighbouring horizontal velocities only, then the value of the pressure in the second layer from top, $P_{i,nj-1}^{n+1}$, can be also defined using the same velocities. Continuing this procedure from layer $nj-1$ to the bottom layer, it can be shown that all of the pressure terms at the time step $n+1$ can be written in the following matrix form:

$$\bar{P}_i = \bar{\bar{R}}_i \bar{U}_{i-1/2} + \bar{\bar{S}}_i \bar{U}_{i+1/2} + \bar{T}_i \tag{15}$$

in which the double overbar denotes a two-dimensional matrix and the single overbar denotes a one-dimensional matrix or vector. The terms $\bar{U}$ and $\bar{P}$ are unknowns representing the u and P values at the time step $n+1$ respectively.

3.3. Creation of a block tri-diagonal system

Equation (12) can now be rewritten in a matrix form giving

$$\bar{\bar{A}}_i \bar{U}_{i-1/2} + \bar{\bar{B}}_1 \bar{P}_i + \bar{\bar{A}}_2 \bar{U}_{i+1} + \bar{\bar{B}}_2 \bar{P}_{i+1} + \bar{\bar{A}}_3 \bar{U}_{i+3/2} = \bar{D}_0 \tag{16}$$

Substituting Equation (15) into Equation (16) reduces the system of equations to a block tri-diagonal matrix system, giving

$$\bar{\bar{A}}_m \bar{U}_{i-1/2} + \bar{\bar{A}}_a \bar{U}_{i+1/2} + \bar{\bar{A}}_p \bar{U}_{i+3/2} = \bar{D}_1 \tag{17}$$

where

$$\bar{\bar{A}}_m = \bar{\bar{A}}_1 + \bar{\bar{B}}_1 \bar{\bar{R}}_i$$

$$\bar{\bar{A}}_a = \bar{\bar{A}}_2 + \bar{\bar{B}}_1 \bar{\bar{S}}_i + \bar{\bar{B}}_2 \bar{\bar{R}}_{i+1}$$

$$\bar{\bar{A}}_p = \bar{\bar{A}}_3 + \bar{\bar{B}}_2 \bar{\bar{S}}_{i+1}$$

$$\bar{D}_1 = \bar{D}_0 - \bar{\bar{B}}_1 \bar{T}_i - \bar{\bar{B}}_2 \bar{T}_{i+1}$$

The block tri-diagonal system (17) was solved using a double sweep algorithm to obtain the horizontal velocity field, with a special treatment being applied for the upstream and downstream boundary conditions. Once the velocity was known, the value of the pressure was obtained using Equation (15).

4. NUMERICAL SCHEME

The algorithm described in Section 3 can be applied to all the three types of sigma co-ordinate grids shown in Figure 1. In this paper, the grid layout shown in Figure 1(c) was deployed, but with only one layer being used in the upper part of the grid (see Figure 2). In this grid system only the thickness of the upper layer varies in time and the thickness of the other layers are divided equally and remain unchanged, so that the accuracy of the scheme is preserved, as the errors associated with the transformation procedure are not included. On the other hand, this limits the application of the scheme to 'nearly horizontal' flow conditions. However, the scope of application of the main algorithm when expressed in a general form is as comprehensive as that of the sigma co-ordinate system.

Details of the numerical scheme applied to this grid system are given below.

4.1. Continuity equation

The continuity equation (1) was discretized around the point (i, j), giving

$$\frac{w^{n+1}_{i,j+1/2} - w^{n+1}_{i,j-1/2}}{\Delta z} + \frac{u^{n+1}_{i+1/2,j} - u^{n+1}_{i-1/2,j}}{\Delta x} = 0 \tag{18}$$

or

$$w^{n+1}_{i,j+1/2} = \frac{\Delta z}{\Delta x} \sum_{k=1}^{j} (u_{i-1/2} - u_{i+1/2})^{n+1}_{k} \tag{19}$$

which is a special form of Equation (10). For the top layer, the continuity equation can be written in the following finite difference form:

$$\frac{\xi^{n+1}_i - \xi^n_i}{\Delta t} + \beta\left(\frac{h_{i+1/2}u^{n+1}_{i+1/2,nj} - h_{i-1/2}u^{n+1}_{i-1/2,nj}}{\Delta x} + w^{n+1}_{i,nj-1/2}\right)$$
$$+ (1-\beta)\left(\frac{h_{i+1/2}u^{n}_{i+1/2,nj} - h_{i-1/2}u^{n}_{i-1/2,nj}}{\Delta x} + w^{n}_{i,nj-1/2}\right) = 0 \tag{20}$$

where $h = \Delta z/2 + \xi^n$ and β is the implicit weighting factor, where $0 < \beta < 1$. Substituting Equation (19) into Equation (20) to eliminate the vertical velocities enables the coefficients in Equation (11) to be determined.

4.2. Vertical momentum equation

Details of the finite difference formulae used in the vertical momentum equation (9) are given as follows:

$$\frac{\partial w}{\partial t} \approx \frac{(w^{n+1} - w^n)_{i,j+1/2}}{\Delta t} \tag{21}$$

$$\frac{\partial(w^2)}{\partial z} = 2w\frac{\partial w}{\partial z} \approx 2w^n_{i,j+1/2}\frac{(w_{j+3/2} - w_{j-1/2})^{n+1}_i}{2\Delta z} \tag{22}$$

$$\frac{\partial(uw)}{\partial x} \approx \frac{w^*_{i+1/2}(u^{n+1}_{i+1/2,j+1} + u^{n+1}_{i+1/2,j}) - w^*_{i-1/2}(u^{n+1}_{i-1/2,j+1} + u^{n+1}_{i-1/2,j})}{2\Delta x},$$

$$w^*_{i\pm 1/2} = \frac{(w^n_i + w^n_{i\pm 1})_{j+1/2}}{2} \tag{23}$$

$$\frac{\partial}{\partial z}\left(\mu\frac{\partial w}{\partial z}\right) \approx \frac{[\mu_{j+1}w^{n+1}_{j+3/2} - (\mu_j + \mu_{j+1})w^{n+1}_{j+1/2} + \mu_j w^{n+1}_{j-1/2}]_i}{(\Delta z)^2} \tag{24}$$

$$\frac{\partial P}{\partial z} \approx \alpha\frac{(P_{j+1} - P_j)^{n+1}_i}{\Delta z} + (1-\alpha)\frac{(P_{j+1} - P_j)^n_i}{\Delta z} \tag{25}$$

$$\frac{\partial}{\partial x}\left(\mu\frac{\partial w}{\partial x}\right) \approx \frac{[\mu^*_{i-1/2}w^n_{i-1} - (\mu^*_{i-1/2} + \mu^*_{i+1/2})w^n_i + \mu^*_{i+1/2}w^n_{i+1}]_{j+1/2}}{(\Delta x)^2},$$

$$\mu^*_{i\pm 1/2,j+1/2} = \frac{\mu_{i,j} + \mu_{i\pm 1,j} + \mu_{i,j+1} + \mu_{i\pm 1,j+1}}{4} \tag{26}$$

where α is the implicit weighting factor, $0 < \alpha < 1$. Equations (22) and (24) can be simplified to give

$$\frac{\partial(w^2)}{\partial z} = 2w\frac{\partial w}{\partial z} = 2w\left(-\frac{\partial u}{\partial x}\right) \approx 2w^n_{i,j+1/2}\frac{u^{n+1}_{i-1/2,j+1} + u^{n+1}_{i-1/2,j} - u^{n+1}_{i+1/2,j+1} - u^{n+1}_{i+1/2,j}}{2\Delta x} \tag{27}$$

$$\frac{\partial}{\partial z}\left(\mu\frac{\partial w}{\partial z}\right) = \frac{\partial}{\partial z}\left(-\mu\frac{\partial u}{\partial x}\right) \approx \frac{[\mu_i(u^{n+1}_{i-1/2} - u^{n+1}_{i+1/2})]_{j+1} - [\mu_i(u^{n+1}_{i-1/2} + u^{n+1}_{i+1/2})]_j}{2\Delta x\ \Delta z} \tag{28}$$

Substituting Equations (27) and (28) into Equation (9) gives

$$P^{n+1}_{i,j} = P^{n+1}_{i,j+1} + f_0 w^{n+1}_{i,j+1/2} + f_1 u^{n+1}_{i-1/2,j+1} + f_2 u^{n+1}_{i-1/2,j} + f_3 u^{n+1}_{i+1/2,j+1} + f_4 w^{n+1}_{i+1/2,j} + f_5 \tag{29}$$

where

$$f_0 = \frac{\Delta z}{\alpha\Delta t}$$

$$f_1 = \frac{\Delta z}{\alpha\Delta x}\left(e w^n_{i,j+1/2} - \frac{w^*_{i-1/2}}{2} - e\frac{\mu_{i,j+1/2}}{\Delta z}\right)$$

$$f_2 = \frac{\Delta z}{\alpha\Delta x}\left(w^n_{i,j+1/2} - \frac{w^*_{i-1/2}}{2} + \frac{\mu_{i,j-1/2}}{\Delta z}\right)$$

$$f_3 = \frac{\Delta z}{\alpha \Delta x}\left(- e w^n_{i,j+1/2} - \frac{w^*_{i+1/2}}{2} + e\,\frac{\mu_{i,j+1/2}}{\Delta z}\right)$$

$$f_4 = \frac{\Delta z}{\alpha \Delta x}\left(- w^n_{i,j+1/2} - \frac{w^*_{i+1/2}}{2} - \frac{\mu_{i,j-1/2}}{\Delta z}\right)$$

$$f_5 = \frac{\Delta z}{\alpha}\left(- \frac{w^n_{i,j+1/2}}{\Delta t} - \frac{[\mu^*_{i-1/2} w^n_{i-1} - (\mu^*_{i-1/2} + \mu^*_{i+1/2}) w^n_i + \mu^*_{i+1/2} w^n_{i+1}]_{j+1/2}}{(\Delta x)^2} + g\right) + \frac{1-\alpha}{a}\,(P^n_{i,j+1} - P^n_{i,j})$$

w^* and μ^* are given in Equations (23) and (26) respectively, and e is defined as

$$e = \tfrac{1}{2} + \xi^n_i/\Delta z \quad \text{for } j = nj$$
$$e = 1 \quad \text{for } j < nj$$

Equation (29) can be rewritten in matrix form as given by Equation (15), with the matrix coefficients $\bar{\bar{R}}_i$, $\bar{\bar{S}}_i$ and $\bar{T}_i$ being determined using the coefficients f_0 to f_5.

4.3. Horizontal momentum equation

The horizontal momentum equation (8) was written for column $i+\frac{1}{2}$ and for row $j = 1, 2, \ldots, nj$, with details of the discretization being given as follows:

$$\frac{\partial u}{\partial t} \approx \frac{(u^{n+1} - u^n)_{i+1/2,j}}{\Delta t} \tag{30}$$

$$\frac{\partial (u^2)}{\partial x} \approx 2u\,\frac{\partial u}{\partial x} \approx 2u^n_{i+1/2,j}\,\frac{(u_{j+3/2} - u_{i-1/2})^{n+1}_j}{2\Delta z} \tag{31}$$

$$\frac{\partial (uw)}{\partial x} \approx \frac{[w^*_{j+1/2}(u^{n+1}_j + u^{n+1}_{j+1}) - w^*_{j-1/2}(u^{n+1}_j + u^{n+1}_{j-1})}{2\Delta x},$$

$$w^*_{i+1/2,j\pm1/2} = \frac{(w^n_{i,j\pm1/2} + w^n_{i+1,j\pm1/2})}{2} \tag{32}$$

$$\frac{\partial}{\partial z}\left(\mu\,\frac{\partial u}{\partial z}\right) \approx \frac{[\mu^*_{j+1/2} u^{n+1}_{j+1} - (\mu^*_{j+1/2} + \mu^*_{j-1}) u^{n+1}_j + \mu^*_{j-1/2} u^{n+1}_{j-1}]_{i+1/2}}{(\Delta z)^2} \tag{33}$$

$$\frac{\partial}{\partial x}\left(\mu\,\frac{\partial u}{\partial x}\right) \approx \frac{[\mu_{i+1} u^{n+1}_{i+3/2} - (\mu_{i+1} + \mu_i) u^{n+1}_{i+1/2} + \mu_{i-1/2} u^{n+1}_{i-1/2}]_j}{(\Delta x)^2},$$

$$\mu^*_{i+1/2,j\pm1/2} = \frac{\mu_{i,j} + \mu_{i+1,j} + \mu_{i,j\pm1} + \mu_{i+1,j\pm1}}{4} \tag{34}$$

$$\frac{\partial P}{\partial x} \approx \gamma \frac{(P_{i+1} - P_i)_j^{n+1}}{\Delta x} + (1-\gamma)\frac{(P_{i+1} - P_i)_j^{n}}{\Delta x} \tag{35}$$

where γ is the implicit weighting factor, $0 < \gamma < 1$.

4.4. Boundary conditions

Wind created shear stress at the water surface can be derived from the local wind speed (u_w) at an elevation of 10 m above the water surface, according to Taylor [9], giving

$$\tau_{xz_s} = C_d \rho_a u_s |u_s| \tag{36}$$

where ρ_a is the air density and C_d is the air–fluid drag coefficient. Hence, the vertical eddy viscosity term at the top layer or (surface layer) can be rewritten as

$$\frac{\partial}{\partial z}\left(\mu \frac{\partial u}{\partial z}\right) \approx \frac{[\tau_{xz_s} - \mu^*_{nj-1/2}(u^{n+1}_{nj} - u^{n+1}_{nj-1})]_{i+1/2}/\Delta z}{(\Delta z)_{av}},$$

$$(\Delta z)_{av} = 0.75\Delta z + 0.5\xi_i^n \tag{37}$$

At the free-surface, the kinematic condition was also used to define the vertical velocity [11], giving

$$w = \frac{\partial \xi}{\partial t} + u\frac{\partial \xi}{\partial x} \tag{38}$$

The free-surface pressure term is defined by Equation (14). At the bed, the bottom shear stress is represented using a quadratic friction law [10]

$$\tau_{xz_b} = r_b u, \quad \text{where } r_b = \rho \frac{g}{C^2}|u| \tag{39}$$

where C is the Chezy bed roughness coefficient.

Equation (39) was then substituted into the bottom layer's momentum equation implicitly, giving

$$\frac{\partial}{\partial z}\left(\mu \frac{\partial u}{\partial z}\right) \approx \frac{[\mu^*_{j+1/2}(u^{n+1}_{j+1} - u^{n+1}_j)/\Delta z - r_b u^{n+1}_j]_{i+1/2}}{\Delta z} \quad \text{for } j = 1 \tag{40}$$

5. MODEL APPLICATIONS

Several numerical tests have been undertaken to test the numerical model and also to investigate the effects of the commonly used hydrostatic pressure distribution assumption on the modelling results. The three tests selected are given below

(i) propagation of a solitary wave,
(ii) propagation of small amplitude Stokes linear waves, and
(iii) formation of a wind-driven velocity field.

5.1. Solitary wave test

In order to test the model behaviour for relatively large free-surface movement, the model was first used to simulate the flow field introduced by a solitary wave. The wave amplitude used in this test was 3 m and the initial water elevation was set to zero. The analytical solutions for the water elevation, depth averaged and vertical velocities are known for this case and can be expressed in the following forms:

$$\xi(x, t) = 4a \frac{\exp(-2\phi(x - ct))}{(1 + \exp(-2\phi(x - ct)))^2} \tag{41}$$

$$v(x, t) = c \frac{\xi(x, t) - h}{\xi(x, t)}, \qquad w(x, z, t) = -\frac{\partial v}{\partial x}(z - z_b) \tag{42}$$

where a is the wave amplitude, h is the mean water depth, c is the wave celerity and ϕ is a coefficient. The wave celerity c and phase ϕ are given as

$$c = \sqrt{g(h + a)}, \qquad \phi = \frac{1}{2h}\sqrt{\frac{3a}{h + a}}$$

The depth-averaged velocity, obtained using Equation (42), was continuously fed into the left boundary. Numerical model predictions have been compared with the above exact solutions, with the numerical parameters selected for this test being: $\Delta x = 4$ m, $\Delta t = 0.2$ s, Δz varies from 1 m to 4 m (i.e. the water depth varies between 15 m and 18 m) for the upper layer and $\Delta z = 2$ m for the other layers. Figure 3(a) shows a comparison of the predicted and analytical water elevations at $t = 40$ s. It can be seen that the variation in the elevations is relatively small. Figure 3(a) also shows excellent agreement between the predicted and analytical wave phase, which means that the wave celerity and velocities were also accurately predicted in the mode. Figure 3(b) shows the velocity and dynamic pressure distribution in the vertical plane. The dynamic pressure was obtained by substituting hydrostatic pressure from the total pressure. It can be seen that, as expected, where the value of the velocity is large then the value of pressure is small, and vice-versa.

5.2. Small amplitude Stokes waves

The second test was to simulate waves propagating from left to right along a 960 m long, 15 m deep wave flume, with the initial water elevation being set zero. A sinusoidal velocity distribution, with its amplitude being 0.3 m s^{-1} at the water surface and zero at the bed, was imposed at the left boundary to simulate the action of the hinge type wave maker. The wave period and theoretical celerity were 4.5 s and 7.02 m s^{-1} respectively. The numerical

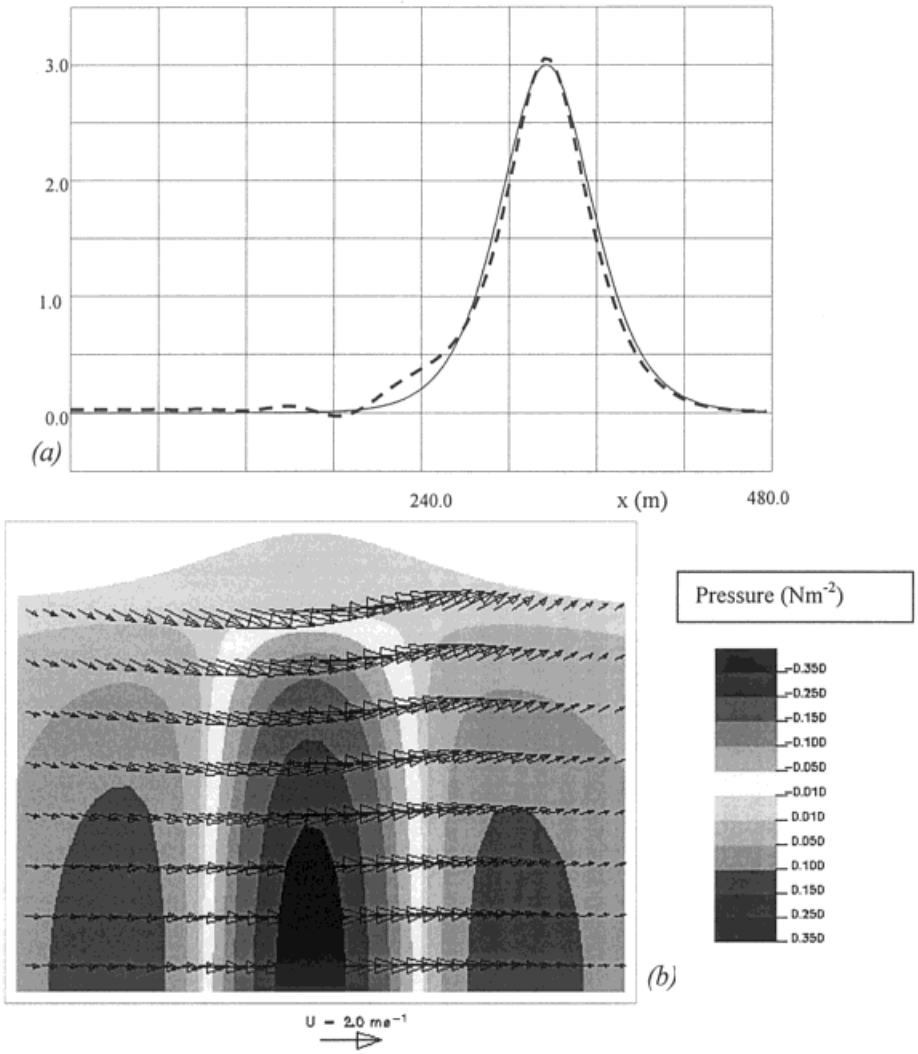

Figure 3. Predicted velocity and pressure distributions for a solitary wave ($t = 40$ s): (a) surface elevations (m), solid line represents analytical solution and dashed line represents model predictions; (b) velocities and dynamic pressure distributions.

parameters used in this test case were: $\Delta x = 4$ m, $\Delta t = 0.2$ s, $\Delta z = 2$ m and with the upper layer varying between 1 m and 4 m.

Figure 4(a) shows the predicted water surface elevation along the first third of the flume, at $t = 135$ s. The predicted wave celerity and the wavelength compare favourably with the corresponding analytical solutions. The wave amplitude of the model results was also predicted

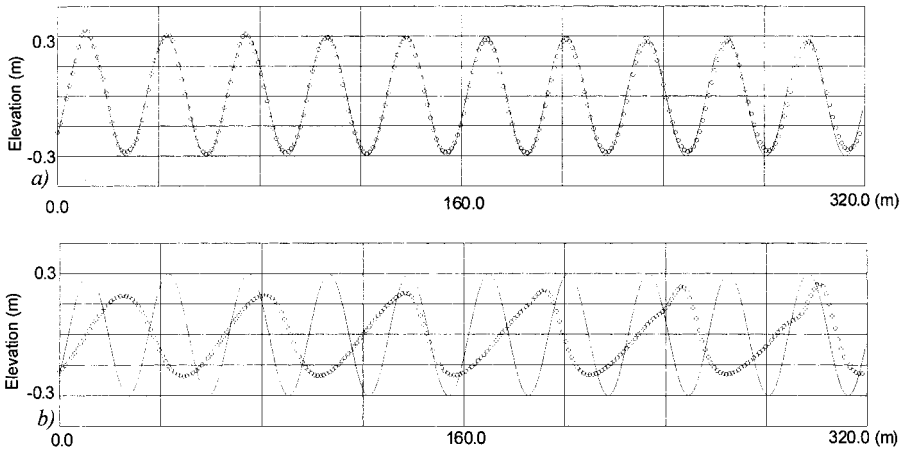

Figure 4. Comparison of water elevations for a small amplitude wave test ($t = 135$ s). Solid line represents analytical solution and dotted line represents model predictions: (a) Model results (with hydrodynamic pressure assumption); (b) no vertical accelerations (with hydrostatic pressure assumption).

satisfactorily. The velocities and the ratio of the top to bottom layer velocities were also shown to be very close to the exact results.Figure 4(b) shows the result of the model with the same initial and boundary conditions but ignoring the vertical acceleration, namely to predict the same flow using a hydrostatic pressure assumption. Large differences in the wave celerity as well as the wave shape can be observed.

5.3. Wind-driven currents

The third test undertaken was to predict the wind-driven circulation in a closed basin. In order to satisfy the mass balance condition, in the upper part of the basin the direction of flow should be in the same direction as the wind, while in the lower part of the basin it should be in the opposite direction (i.e. the classic 'conveyor belt' structure). Thus, the vertical acceleration at the two extremes of the basin plays an important role in generating this circulation. The mean water depth and wind speed used for this test case were 30 m and 10.0 m s^{-1} respectively. The numerical parameters selected for this test case were: $\Delta x = 2$ m, $\Delta t = 0.5$ s, $\Delta z = 2$ m and basin depth $= 30$ m.

A comparison of the model predictions was undertaken both with and without vertical acceleration terms, while all other conditions were kept the same. The predicted velocity fields for these two cases are shown in Figure 5(a) and (b) respectively. It can be seen that in using the hydrostatic pressure assumption a very rapid change of the velocity direction occurs near the right hand boundary, which then introduces minor velocity oscillations in the region. This phenomenon has also been observed when a layer integrated three-dimensional model was used to simulate the same problem [3], and where the hydrostatic pressure assumption was used. Using the hydrodynamic assumption, the change in the velocity direction is much

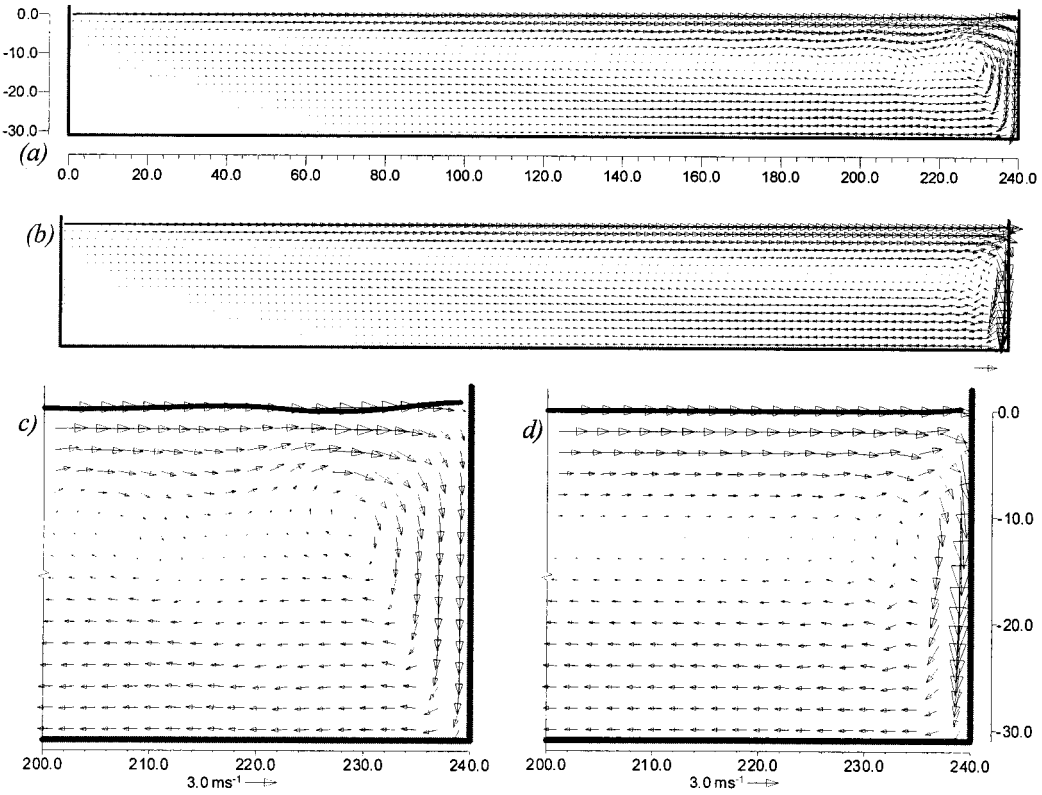

Figure 5. Predicted velocity distributions ifor a wind driven flow with and without vertical accelerations: (a) and (c) with vertical acceleration; (b) and (d) without vertical acceleration.

smoother and the oscillations of the velocity vectors have disappeared, see Figure 5(b). This indicates that where a strong vertical acceleration exists, then the hydrodynamic pressure representation is needed.

As discussed in Section 4, some implicit parameters have been introduced in the numerical discretisation. From the numerical tests it has been observed that: (a) for modelling short waves, the minimum phase and amplitude error occurred when those parameters were close to 0.5; and (b) for modelling long waves and or steady flows, the higher values of the parameters gave more stable solutions.

6. CONCLUSION

Details of a novel numerical algorithm for modelling free-surface flows using the full vertical momentum equations have been presented. Using this algorithm, water elevation, pressure and

velocity field can be predicted simultaneously. Since the vertical momentum equation is treated in the same way as the horizontal momentum equation, the model can be used to predict free-surface flows with considerable vertical accelerations.

The numerical algorithm was designed for general sigma co-ordinate grids. Although three types of sigma co-ordinate grids were discussed in the paper, the tests considered herein were only applied to one type of grid. Implicit finite difference schemes were used to discretize the governing equations and the finite difference equations generated were arranged in a block tri-diagonal matrix form so that no iteration was required for solving these equations.

Since both the vertical acceleration and the water surface elevation are of considerable significance in short wave cases, two of the numerical tests undertaken were to simulate short period waves. Detailed comparisons showed that the model was able to represent accurately the free-surface elevation, and the pressure and velocity distributions. Numerical tests also showed the importance of using the non-hydrostatic pressure representation when the magnitude of vertical accelerations was of same order of magnitude as those in the horizontal plane. The corresponding predictions of the velocity field for a wind circulation in an idealized rectangular reservoir showed a marked difference when the non-hydrostatic pressure representation was used, with the hydrostatic pressure assumption model giving spurious results.

Although the model presented in this paper is for two-dimensional flows in the vertical plane, it can be extended to model three-dimensional flows. Such a modification is currently being undertaken by the authors.

ACKNOWLEDGMENTS

This first author would like to thank the sponsorship given by the State Scientific Research Council (Iran, project number 2827).

REFERENCES

1. Cheng RT, Smith PE. A survey of three-dimensional numerical estuarine models. In *Estuarine and Coastal Modelling Proceedings*, Spaulding. ASCE: Newport, 1989; 235–280.
2. Stelling GS, van Kester JA. On the approximation of horizontal gradients in sigma co-ordinates for bathymetry with steep bottom slopes. *International Journal for Numerical Methods in Fluids* 1994; **18**: 915–935.
3. Lin B, Falconer RA. Three-dimensional layer integrated modelling of estuarine flows with flooding and drying. *Estuarine, Coastal and Shelf Science* 1997; **44**: 737–751.
4. Stansby PK, Zhou JG. Shallow-water flow solver with non-hydrostatic pressure: 2D vertical plane problems. *International Journal for Numerical Methods in Fluids* 1998; **28**: 541–563.
5. Casulli V, Stelling GS. Numerical simulation of 3D quasi-hydrostatic, free-surface flows. *Journal of Hydraulic Engineering, ASCE* 1998; **124**: 678–686.
6. Perrels PA, Karelss JM. A two-dimensional laterally averaged model for salt intrusion in estuaries. Delft Hydraulics Publication No. 262, 1982; 483–535.
7. Zhou JG. Velocity-depth coupling in shallow-water flows. *Journal of Hydraulic Engineering, ASCE* 1995; **121**: 717–724.
8. Ouillion S, Dartus D. Three-dimensional computation of flow around Groyne. *Journal of Hydraulic Engineering, ASCE* 1997; **123**: 962–970.
9. Taylor GI. Skin friction of the wind on the earth's surface. *Proceeding of Royal Society London* 1916; **92**: 196–199.

10. Henderson FM. *Open Channel Flow*. Collier MacMillan: London, 1966.
11. Ghiassi R. Three dimensional coastal flow modelling using the finite volume method. PhD thesis, University of Bradford, UK, 1995.
12. Hirt CW, Nichols BD. Volume of fluid (VOF) method for the dynamic of free boundaries. *Journal of Computational Physics* 1981; **39**: 201–255.
13. Smagorinsky JS. General circulation experiments with the primitive equations: part I. Basic experiments. *Monthly Weather Review* 1963; **91**: 99–164.

